Particle transport by a vortex soliton

By Y. KIMURA[1] AND S. KOIKARI[2]

[1]Graduate School of Mathematics, Nagoya University, Furo-cho, Chikusa-ku, Nagoya 464-8602, Japan

[2]Department of Mechanical Engineering, Graduate School of Engineering, Kyoto University, Yoshida-Honmachi, Sakyo-ku, Kyoto 606-8501 Japan

Motions of fluid particles advected by a vortex soliton are studied. In a reference frame which moves with the vortex soliton, particle motions are confined in a torus near the loop part of the vortex soliton for a wide range of three parameters that characterize the shape and strength of the vortex soliton. The transported volume is calculated numerically as a function of these parameters. The product of the volume and the translational velocity of the soliton provides the rate of transport. Using this quantity, the optimized shape of the soliton for the maximum rate of transport is considered. The torus is composed of groups of invariant surfaces around periodic trajectories. Similar phenomena are observed with the KAM tori for non-integrable Hamiltonian systems. To extract the essential mechanism of the transport properties, an ordinary differential equation model is proposed, which is named the 'chopsticks model'. This model successfully explains the qualitative features of the transport.

1. Introduction

Transport of fluid particles by an isolated vortex has been a fundamental problem which, particularly if a vortex moves steadily, provides a direct example of long-surviving advection of materials in fluids. In this context, we can use the transport of fluid volume by a vortex ring as an example. Batchelor (1967) showed types of closed streamlines relative to a thin vortex ring as a function of the parameter ϵ/a, where ϵ is the core radius and a is the curvature radius of the vortex ring. (The appearance of such a parameter ϵ/a in the discussion of motion of a thin curved vortex is endemic because the asymptotic velocity as $\epsilon \to 0$ in the Biot-Savart integral has a term proportional to $\log(a/\epsilon)/a$, and thus velocity diverges for a vortex filament with zero radius.) From the viewpoint of transport, the volume surrounded by the outermost closed streamlines is the quantity carried by the vortex ring, which can be evaluated by means of the elliptic integrals. This situation can be extended to any two-dimensional steady flow fields including axisymmetric ones so that existence of closed streamlines always indicates existence of trapped fluid particles inside, which amounts to finite transport volume (Batchelor 1956; Kraichnan 1970; Rhines & Young 1983). Furthermore, if we recall that a two-dimensional incompressible flow is always equivalent to a Hamilton dynamical system of one degree of freedom with the streamfunction, $\psi(x, y)$, as Hamiltonian (Aref 1991), and that there are always closed level curves, $\psi(x, y) = c$, around an elliptic fixed point, we have a finite-volume transport if there is an elliptic fixed point in two-dimensional flows. For finding fixed points in two-dimensional vector fields, in general, methods such as calculation of rotation number can be used (Grimshaw 1990).

The main objective of this paper is to demonstrate an example of finite-volume transport by a three-dimensional thin steady vortex tube, called a vortex soliton named by Hasimoto (1972). The vortex soliton is one of the few steady solutions for a vortex filament under the local induction approximation moving without changing its shape (Kida 1981). The original observation of a vortex soliton in a rotating tank experiment implies that a vortex soliton is endowed with the ability to transport physical quantities, such as mass, kinetic energy, and linear and angular momenta, from a turbulent region to a laminar one (Hopfinger & Browand 1982; Hopfinger, Browand & Gagne 1982). In fact, transport of impulse and angular momentum by a vortex soliton was calculated by one of the present authors, and as a direct application of this result, the sound pressure in a far field based on the Lighthill vortex sound theory could be derived (Kimura 1989). Later, the result was extended to the case of two soliton interaction (Konno & Ichikawa 1995). Among others, mass is the most fundamental and important quantity in the transport phenomena of the vortex soliton, which has not been investigated.

As we shall see in the subsequent sections, the flow structure is much more complicated in three-dimensional in contrast with two-dimensional flow fields. For example, in place of a fixed point and surrounding closed orbits for two-dimensional flows, a periodic orbit and surrounding invariant tori play central roles for the transport in a three-dimensional vortex system. Unfortunately, there is no known systematic method for finding a periodic orbit in a vector field, and thus hunting for a periodic orbit is always associated with serendipity. We could verify numerically, however, that there is at least one periodic orbit twining around the vortex core near the loop of the soliton for a wide range of parameters which characterize the shape of the soliton, and that invariant tori with finite volume surround the periodic orbit. The structure and properties of the tori are investigated by using Poincaré sections and calculating the winding numbers (Lichtenberg & Lieberman 1983). We could find similarity between the KAM tori for non-integrable Hamiltonian systems.

The organization of the paper is as follows: the formulation and the methodology are presented in §2. In §3, we shall show the numerical results on the transported volume for various combinations of parameter values for the soliton and on the topological properties of the invariant tori. Finally, discussion is given in §4 where we present a simplified model equation, the 'chopsticks model' to explain the mechanism of the chaotic and integrable motion of particles around the vortex soliton.

2. Formulation

2.1. *Vortex soliton*

The Hasimoto vortex soliton is a solitary wave-type solution of the localized induction equation (LIE) for the motion of an isolated vortex filament,

$$\frac{\partial \mathbf{X}}{\partial t} = \frac{\Gamma}{4\pi} \log\left(\frac{L}{\epsilon}\right)\left(\frac{\partial \mathbf{X}}{\partial s} \times \frac{\partial^2 \mathbf{X}}{\partial s^2}\right), \tag{2.1}$$

where $\mathbf{X}(s, t)$ is the position of the centreline of the filament parameterized by the arc length s and time t. In (2.1), L and ϵ are two cutoff lengths, large and small, respectively, and Γ is the circulation which is defined as a line integral of velocity vector $\mathbf{v}$ along a loop c around the vortex filament. By means of the Stokes theorem, Γ can be evaluated as the surface integral of vorticity vector $\boldsymbol{\omega}$ over the surface S

bounded by the closed curve c,

$$\Gamma = \oint_c \boldsymbol{v} \cdot \mathrm{d}\boldsymbol{x} = \int_S \boldsymbol{\omega} \cdot \boldsymbol{n} \, \mathrm{d}A.$$

The essential idea in deriving the LIE is to desingularize the Biot-Savart integral for velocity around a vortex tube using the two cutoff length scales, L and ϵ (Hama 1962, 1963). The physical meanings these scales have are, negligence of the long-distance effect on the self-induced motion for the former, and assumption that the filament is thin with the constant core radius which can be approximated by the latter. Readers interested in the history and derivation of the LIE should refer to the textbooks: Batchelor (1967); Lamb (1980); Saffman (1992); Newton (2001) and review articles: Leonard (1985); Majda (1991); Ricca (1991).

The secondary assumption attached to the derivation of the LIE is to set the logarithmic self-induction coefficient in (2.1), a constant which is usually removed by rescaling time. Hereinafter, however, we leave it as $G > 0$ in the equation. The reasons for this are (i) to keep the consistency of time with that for the vortex filament and that for the advected particles, and (ii) (following Batchelor) to investigate the topological features of the flow field around the vortex as a function of the parameter. Thus, our equation for the motion of the vortex tube is

$$\frac{\partial \boldsymbol{X}}{\partial t} = G \, \frac{\partial \boldsymbol{X}}{\partial s} \times \frac{\partial^2 \boldsymbol{X}}{\partial s^2}. \tag{2.2}$$

Following Hasimoto (1972), the soliton solution for (2.2) is given with two additional parameters $\nu > 0$ and τ, where ν is related to the curvature of a soliton $\kappa(s)$ by the formula $\kappa(s) = 2\nu \operatorname{sech}(\nu s)$ and τ is the constant torsion of a soliton. By denoting $\boldsymbol{X}(s, t) = {}^t(X_f(s, t), Y_f(s, t), Z_f(s, t))$, we obtain

$$\left. \begin{aligned} X_f(s, t) &= \frac{2\mu}{\nu} \operatorname{sech}\{\nu(s - 2\tau Gt)\} \cos\{\tau(s - 2\tau Gt) + (\nu^2 + \tau^2)Gt\}, \\ Y_f(s, t) &= \frac{2\mu}{\nu} \operatorname{sech}\{\nu(s - 2\tau Gt)\} \sin\{\tau(s - 2\tau Gt) + (\nu^2 + \tau^2)Gt\}, \\ Z_f(s, t) &= s - \frac{2\mu}{\nu} \tanh\{\nu(s - 2\tau Gt)\}, \end{aligned} \right\} \tag{2.3}$$

where $\mu = \nu^2/(\nu^2 + \tau^2)$.

The motion of the Hasimoto vortex soliton consists of rotation around a fixed axis (with a constant angular velocity) and translation (with a constant linear velocity) of one space curve of infinite length. Kida (1981) contrarily used this condition of congruent transformation upon the LIE as a criterion to characterize a class of vortex filament solutions without deforming their shape which includes the Hasimoto vortex soliton. We can verify this property by writing the solution (2.3) as

$$\boldsymbol{X}(s, t) = \boldsymbol{A}(t)\boldsymbol{x}(\sigma) + \boldsymbol{b}(t), \tag{2.4}$$

where $\boldsymbol{x}(\sigma) = \boldsymbol{X}(\sigma, 0)$, namely $\boldsymbol{x}(\sigma) = {}^t(x_f(\sigma), y_f(\sigma), z_f(\sigma))$ where

$$\left. \begin{aligned} x_f(\sigma) &= \frac{2\mu}{\nu} \operatorname{sech}(\nu\sigma) \cos(\tau\sigma), \\ y_f(\sigma) &= \frac{2\mu}{\nu} \operatorname{sech}(\nu\sigma) \sin(\tau\sigma), \\ z_f(\sigma) &= \sigma - \frac{2\mu}{\nu} \tanh(\nu\sigma), \end{aligned} \right\} \tag{2.5}$$

and $\sigma = s - 2\tau Gt$. The pair of congruent transformation $(\boldsymbol{A}, \boldsymbol{b})$ is defined as

$$\boldsymbol{A}(t) = \begin{pmatrix} \cos(\omega t) & -\sin(\omega t) & 0 \\ \sin(\omega t) & \cos(\omega t) & 0 \\ 0 & 0 & 1 \end{pmatrix}, \quad \boldsymbol{b}(t) = \begin{pmatrix} 0 \\ 0 \\ 2\tau Gt \end{pmatrix}, \tag{2.6}$$

where $\omega = (\nu^2 + \tau^2)G$.

2.2. Particle motion

We assume that fluid particles are advected by the velocity induced by the vortex soliton through the Biot-Savart integral taken over the centreline of the vortex tube. Under this assumption, the equation of motion of a fluid particle in the laboratory frame is

$$\frac{\mathrm{d}\boldsymbol{R}}{\mathrm{d}t} = \frac{\Gamma}{4\pi} \int_{-\infty}^{\infty} \frac{\boldsymbol{X}'(s, t) \times (\boldsymbol{R} - \boldsymbol{X}(s, t))}{|\boldsymbol{R} - \boldsymbol{X}(s, t)|^3} \, \mathrm{d}s, \tag{2.7}$$

where $\boldsymbol{R}(t) = {}^t(X(t), Y(t), Z(t))$ denotes the position of a particle, and $\boldsymbol{X}(s, t)$ is the solution of the vortex soliton (2.6). By substituting (2.4) as well as $\boldsymbol{R} = A(t)\boldsymbol{r} + \boldsymbol{b}(t)$, into (2.7), we can introduce a moving frame on which the vortex soliton is kept still where $\boldsymbol{r} = {}^t(x(t), y(t), z(t))$ is the position of the particles observed from the moving frame.

By making use of the relations such as $\mathrm{d}\boldsymbol{R}/\mathrm{d}t = (\mathrm{d}A/\mathrm{d}t)\boldsymbol{r} + \boldsymbol{A}\mathrm{d}\boldsymbol{r}/\mathrm{d}t + \mathrm{d}\boldsymbol{b}/\mathrm{d}t$ and the fact that $\boldsymbol{A}$ is an orthogonal matrix, we obtain

$$\frac{\mathrm{d}\boldsymbol{r}}{\mathrm{d}t} = \frac{1}{4\pi} \int_{-\infty}^{\infty} \frac{\boldsymbol{x}'(s) \times (\boldsymbol{r} - \boldsymbol{x}(s))}{|\boldsymbol{r} - \boldsymbol{x}(s)|^3} \, \mathrm{d}s + \omega \begin{pmatrix} y \\ -x \\ 0 \end{pmatrix} + \begin{pmatrix} 0 \\ 0 \\ -2\tau G \end{pmatrix}. \tag{2.8}$$

In (2.8), we have eliminated the circulation Γ by a suitable choice of time scale and redefined the symbols $G/\Gamma \to G$ and $\omega/\Gamma \to \omega$. We employ (2.8) as an autonomous dynamical system for the motion of particles around the vortex soliton. The solution to (2.8) with an initial condition ${}^t(x(0), y(0), z(0))$ provides a triplet ${}^t(x(t), y(t), z(t))$ which defines a trajectory in the three-dimensional phase space. Notice that the second and the third terms on the right-hand side compensate for the rotation and the translation, respectively, to make the vortex soliton steady.

Equation (2.8) possesses some scaling property and symmetry for parameters ν and τ which enable us to reduce the parameter space for investigation of the solutions. We can verify that if $\tilde{\boldsymbol{r}}(t)$ is a solution of (2.8) with the parameters $(\alpha\nu, \alpha\tau)$, then $\boldsymbol{r}(\xi = \alpha^2 t) \equiv \alpha\tilde{\boldsymbol{r}}(t)$ is also a solution with (ν, τ). In other words, the geometrical properties of the solution such as the shapes of trajectories of particles are completely specified by the ratio of ν to τ. In addition to the ratio, we use a condition, $2\mu/\nu = 2\nu/(\nu^2 + \tau^2) = 1$ to determine the values of ν and τ, which imposes an auxiliary condition that the diameter of the loop is always 1.

Also, we can see that if $\boldsymbol{r}(t) = {}^t(x(t), y(t), z(t))$ is a solution with (ν, τ), $\boldsymbol{r}(t) = {}^t(x(t), y(t), -z(t))$ is a solution with $(\nu, -\tau)$. Using this symmetry, we can restrict τ to the positive without loss of generality.

Another property that the right-hand side of (2.8) holds is the reversible symmetry by Moser (1973): the right-hand side, if denoted $\boldsymbol{u}(\boldsymbol{x})$, satisfies a relation $\boldsymbol{u}(\boldsymbol{A}\boldsymbol{x}) = -\boldsymbol{A}\,\boldsymbol{u}(\boldsymbol{x})$ concerning with a linear transformation $\boldsymbol{A} = \mathrm{diag}(1, -1, -1)$. The transformation has a property that $\boldsymbol{A}^2 = id$. (We should notice that this symmetry is
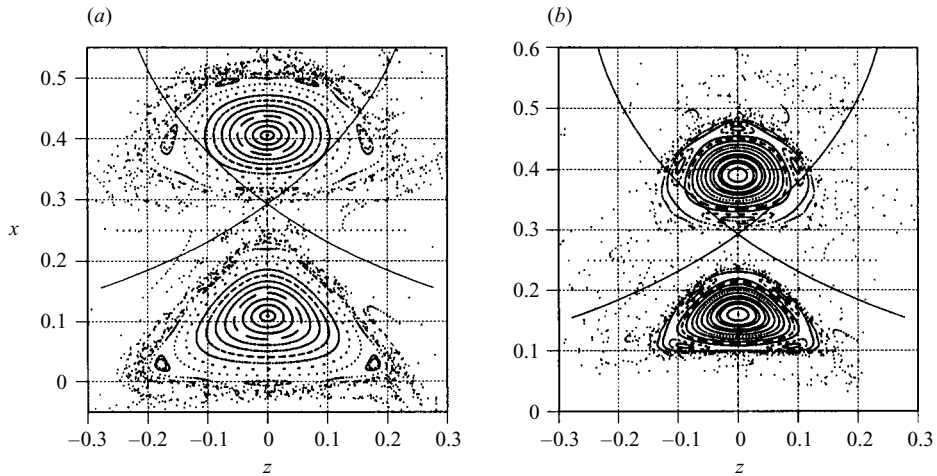
FIGURE 1. Poincaré sections for trajectories of (2.8) with various initial conditions. The Poincaré plane is located at $y = 0$. The parameter values are $(\nu, \tau) = (1.924, 0.3827)$ and (*a*) $G = 0.1832$, (*b*) $G = 0.3113$. The solid lines indicate the vortex soliton projected onto the plane.

an extension of the symmetry for a Hamiltonian system of n degrees of freedom. For the latter case, the same relation holds with $\boldsymbol{A} = \mathrm{diag}(\underbrace{1, \ldots, 1}_{n}, \underbrace{-1, \ldots, -1}_{n})$.)

For the numerical technique to evaluate the integral part in (2.8), first we divided the integration range from $(-\infty, \infty)$ to $[-L, L] + (-\infty - L] \cup [L, \infty)$ where the range $[-L, L]$ is determined so that the velocity induced by the vortex tube outside this range would be equivalent with the velocity that would be induced by a tentative straight vortex filament replacing the vortex tube. Then, the range $[-L, L]$ is divided into small segments and the formula with a Gauss–Legendre polynomial of the seventh order is used for each interval for integration. For the time marching for (2.8), the fifth-order Runge–Kutta–Fehlberg formula with six stages is used.

3. Numerical results

As a canonical tool to analyse trajectories in a phase space of higher dimension than two, the Poincaré section is well known. Figure 1 shows the Poincaré sections for the trajectories of (2.8) with various initial conditions for two different values of G (0.1832 and 0.3113). The Poincaré plane is located at $y = 0$, and a dot is placed at a point on the plane every time a trajectory passes the plane transversally at the point (Lichtenberg & Lieberman 1983).

On both the Poincaré sections, we can see that there are two large islands of groups of nested curves (composed of continuous and broken lines) surrounded by small islands and scattered points. Each large island has a centre which corresponds to a single periodic orbit in the original three-dimensional space. Each nested curve around the centre point, on the other hand, corresponds to an invariant torus around the periodic orbit. The scattered points outside the islands show the trajectories of particles flown apart from the loop by the uniform translational flow in the moving frame.

The difference in G affects the size of the area of the large islands and the number of secondary islands. From (2.8), on the other hand, we see that changing G results in changing the translational and the rotational speed of the soliton. The change in
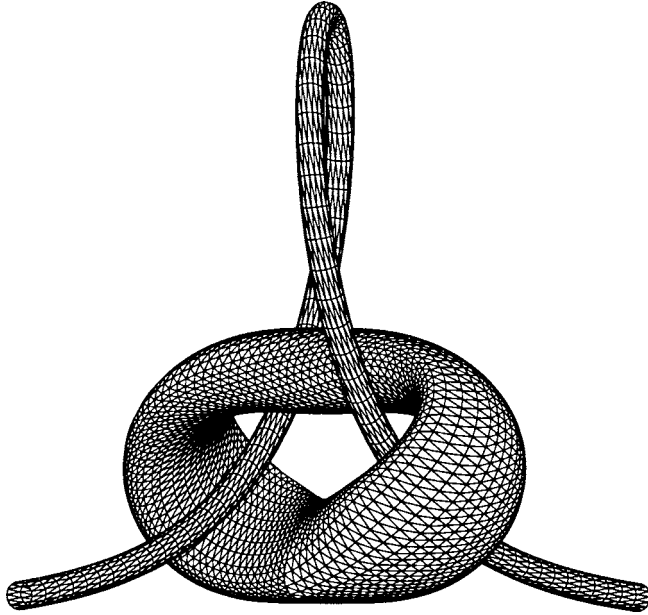
FIGURE 2. Perspective view of a torus with the vortex soliton for $(\nu, \tau) = (1.924, 0.3827)$ and $G = 0.1832$. The torus forms a knot with the loop part of the soliton.

the translation speed seems to cause the change in the area of the island while the change in the rotation speed seems to produce the change of the twisting rate, or the poloidal periodicity of the trajectories. We shall see the detail of these points later.

To understand the torus structure in three-dimension, we show a perspective view of one surface of the torus with the vortex soliton in figure 2. The surface is drawn with a net pattern whose threads in the toroidal direction are made of one particle trajectory on the torus. It can be observed that the trajectory moves on the torus while being twisted, and this twist suggests a non-zero winding number for the trajectory. As a whole, the twisted torus makes a knot with the loop part of the vortex soliton.

To see the structure of the tori in detail, the two levels of enlargement of figure 1 are presented in figure 3 ($(a), (c)$ $G = 0.1832$, $(b), (d)$ $G = 0.3113$). The broken lines in figure 1 are connected so that each layer can be identified clearly. The upper figures, showing only the left half because of the symmetry, are primarily to visualize the main and secondary islands. For smaller G, there are 5 secondary islands (figure 3a) whereas for the larger G there are 4 in a smaller more compact and round shaped region (figure 3b). (Notice that the magnification is different.) The further magnified views of other parts of the Poincaré sections are shown in figures 3(c) and 3(d). Both the figures show a hierarchical structure of smaller islands in a stochastic sea of scattered points near the hyperbolic point between the secondary islands. These features of chaos in the Poincaré sections, such as stochastic layers or the Poincaré–Birkoff chain of islands, are similar to those for KAM tori for non-integrable Hamiltonian systems even though the present system is three-dimensional and not a Hamiltonian (cf. § 5).

As a quantity to characterize the properties of the tori, plots of the winding number for the two values of G are presented in figure 4. Here, the winding number is defined
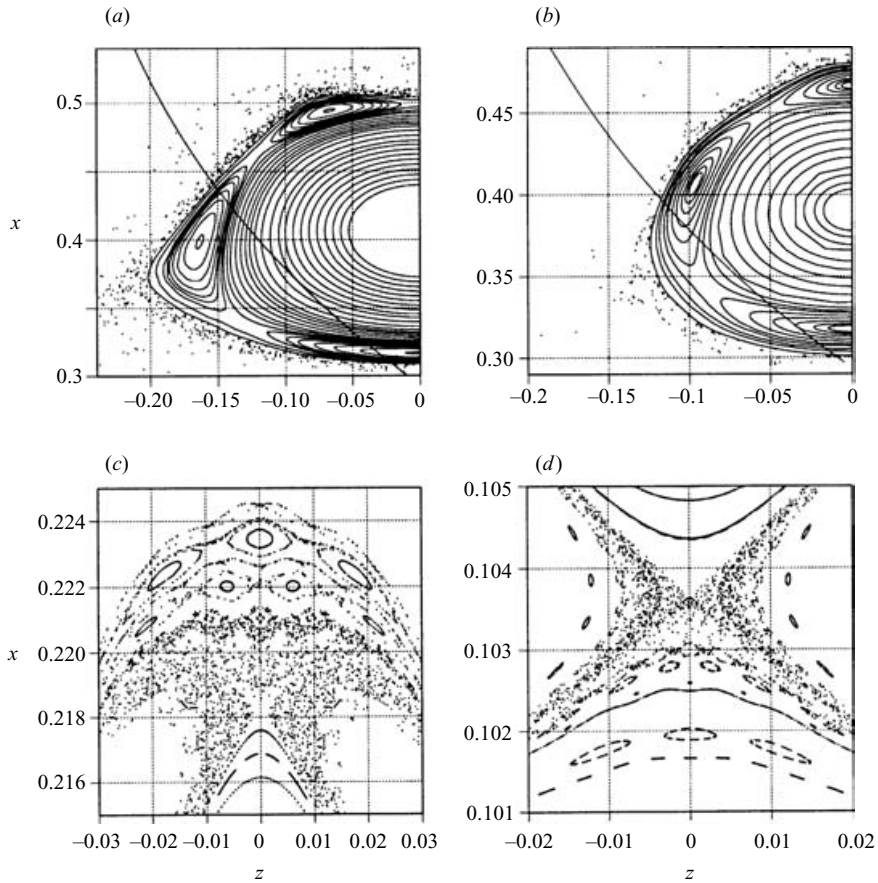
FIGURE 3. Enlargement of Poincaré sections for (2.8) for $(v, \tau) = (1.924, 0.3827)$ with (a, c) $G = 0.1832$ and (b, d) $G = 0.3113$. Only the left half is drawn for the above figures because of the symmetry.
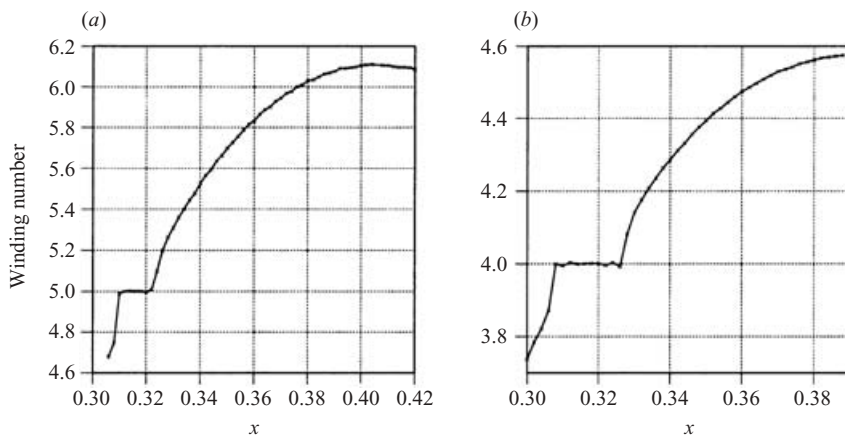

FIGURE 4. Winding numbers W calculated by the formula (3.1) for (a) $G = 0.1832$ and (b) $G = 0.3113$. The inverses of the values are plotted so that closed orbits with a period n give a value n. The plateau in W occurs because range of angles is restricted in the secondary island.

as

$$W = \lim_{N\to\infty} \left[\frac{1}{2\pi N} \sum_{n=1}^{N} (f^n(\theta) - f^{n-1}(\theta)) \right], \tag{3.1}$$

where $f(\theta)$ is the map of the polar angle variable measured with the period 1 orbit at the centre in one (toroidal) period (circle map). The meaning of the winding number is the average increase in the angle θ per toroidal period, or, in other words, the ratio between the poloidal and toroidal periods ω_P and ω_T. The winding number is calculated for each trajectory with an initial condition $(x, z) = (x, 0)$ for varying x. (The graphs are plotted after taking the inverses so that closed orbits with a period n give a value n). Each (surface of the) torus seems to have a specific winding number except for an interval of x where the winding numbers have a plateau which corresponds to the region of a secondary island of tori. The varying winding number in the group of the primary island of tori indicates a differential rotation inside, which may cause a source of rapid mixing of materials inside the island. The plateau of W, namely 1/5 for $G = 0.1832$ and 1/4 for $G = 0.3113$, occurs because the range of the angle is restricted in the secondary island. If the winding number ought to be defined for a mapping from S^1 to S^1, W should be calculated with an nth iterated map for an island which has an n periodic orbit as its centre, and the angle should be measured from the centre.

The most interesting and fundamental quantity of the transport by the vortex soliton is the fluid mass which can be estimated by calculating the volume surrounded by the outermost torus. As we saw in figure 1, the cross-section of a torus has a different area according to the parameters (ν, τ, G), and so does the transported volume. First, figure 5(a) shows the range of parameter values for which a torus with a finite volume is observed numerically. The crosses indicate the parameter values of τ and G which allow a torus. Notice that we have imposed a relation $2\nu/(\nu^2 + \tau^2) = 1$ to make the size of the loop part almost 1. From this relation with the reality condition for ν and τ, we have $0 < \nu < 2$, $-1 < \tau < 1$. Only the result for $0 < \tau < 1$ is demonstrated in figure 5(a) because of a symmetry in τ, but we can expect a torus for $-1 < \tau < 0$ also. There is a clear boundary for the existence of a torus which is drawn as a solid line in the figure. Also, we can see that a smaller G has a wider range of τ for the existence of a torus, or, in other words, the torus structure is robust for smaller values of G.

Next, figure 5(b) shows the volume of the torus as a function of G for several pairs of ν and τ. The robustness for smaller G is endorsed by the large volume for any combination of ν and τ. For a given G, a larger value of ν (which means a smaller τ) always gives a larger value of the volume. However, the dependence of the volume on G becomes weaker for larger ν (smaller τ) which implies that the transported volume is determined only by the shape of a vortex soliton asymptotically as $\nu \to 2$ ($\tau \to 0$) which corresponds to a loop on a plane. To grasp the change in the shape of the soliton according to ν and τ, we plotted three-dimensional figures of solitons in figure 5(c) for some pairs of ν and τ chosen from those used in figure 5(a, b). The loop structure and the two-dimensionality are more obvious for solitons with larger ν (and smaller τ), and these solitons transport more volumes. It should be pointed out, however, that the soliton with a smaller τ translates with slower velocity, and thus if we are concerned with the rate of transport which maybe evaluated as (volume) $\times$ (velocity), there should be optimized values of ν and τ for the maximum rate of transport. In figure 6(a), we plotted this quantity, (volume) $\times$ (velocity), making use of the data in figure 5(b). We can verify that the case with the smallest τ in figure 5(b)
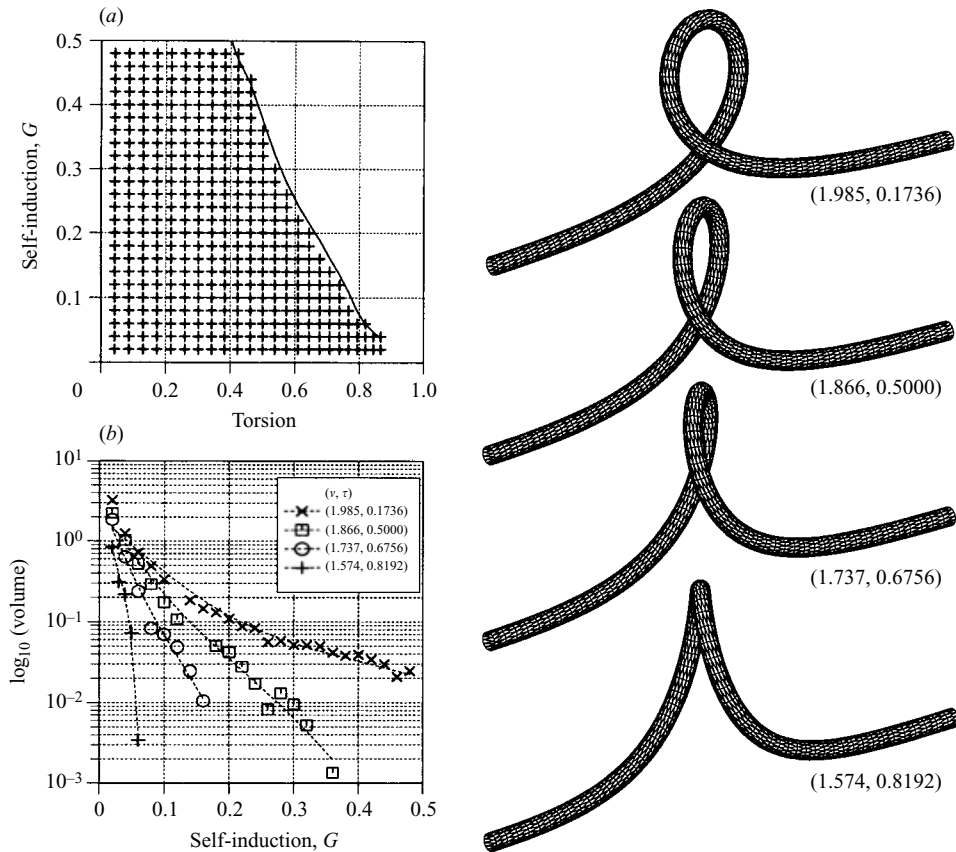
FIGURE 5. (*a*) Range of parameter values for which a torus with a finite volume is observed numerically. There is a clear boundary for the existence of a torus with a finite volume. (*b*) Volume of the outermost torus as a function of G for various combinations of (ν, τ). The volume is a monotonously decreasing function of G, but the rate of decrease is smaller for smaller τ which corresponds to a more planar loop vortex. (*c*) Change in the shape of the soliton according to the combinations of (ν, τ) in (*a*) and (*b*). The loop is more planar for smaller τ.

has a lower rate of transport than some other cases with larger τ in the region of smaller G. Another case of ν and τ is added to the figure for which we could obtain almost the maximum rate of transport throughout all G. The corresponding shape of the soliton is plotted in figure 6(*b*). We can assert that this is a shape close to the optimized vortex soliton for the maximum rate of transport.

To understand and extract the essential mechanism of the formation of tori and the appearance of chaos as well as the transport of volume, we calculated trajectories of particles for a truncated model system of a vortex soliton in which only some parts of the filament have a non-zero contribution to the Biot-Savart integral in (2.8) (leaving other terms unchanged.) Figure 7 shows the Poincaré section and the three-dimensional perspective view of one torus with the vortex soliton whose non-zero circulation parts are drawn by solid lines. The parameter values are $(\nu, \tau, G) = (1.924, 0.3827, 0.1832)$ which correspond to figure 1(*a*). Only small portions of the loop filament can produce the qualitatively similar structure of tori
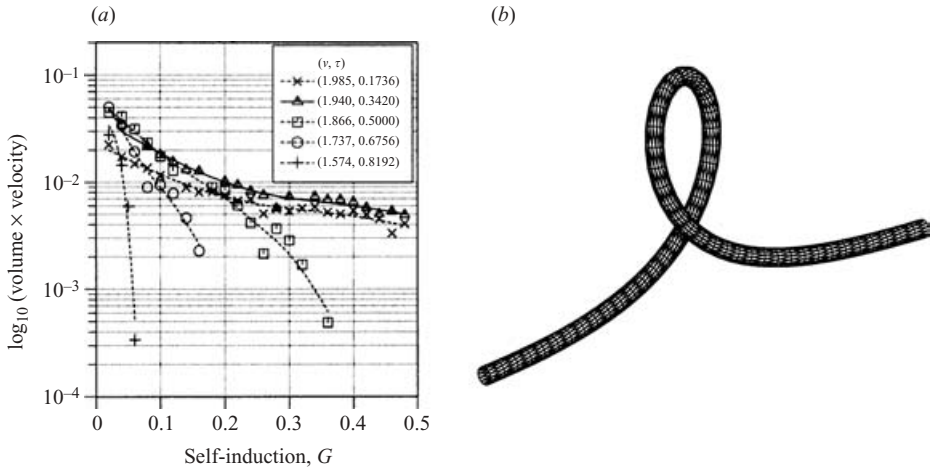
FIGURE 6. (*a*) Plot of the rate of transport, (volume) × (velocity) from the data in figure 5(*b*). The case with the smallest τ in figure 5(*b*) (×), which had the maximum transported volume, has a lower rate of transport than some other cases with larger τ in the region of smaller G. Another case of ν and τ (Δ) is added which shows almost the maximum rate of transport throughout all G. (*b*) The corresponding shape of the soliton for almost the maximum rate of transport.
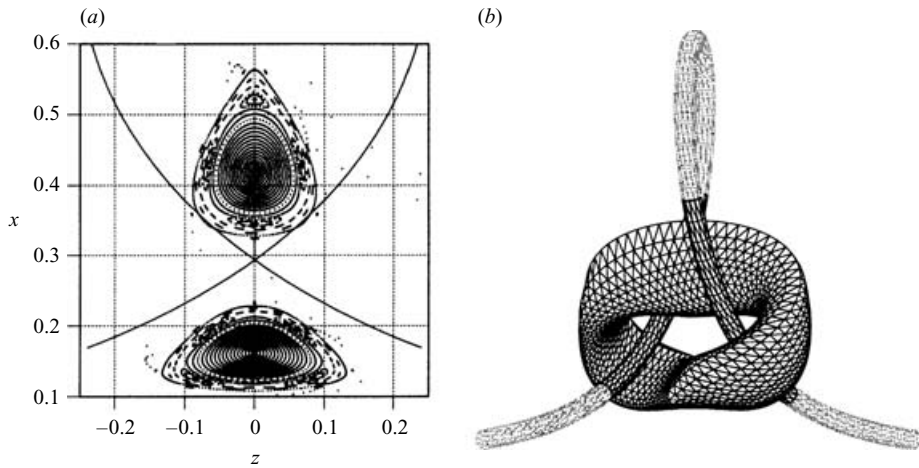

FIGURE 7. Poincaré section and perspective view of a torus made by the truncated vortex model. The part with non-zero circulation is drawn with a thick lines. All other parts are neglected for calculating the Biot-Savart integral.

(both primary and secondary). We observe that the upper part of the tori is extended upward perhaps because of the non-existence of the loop part, but the more important thing is that the loop structure is not essential for making the tori.

The success of reproducing the torus structure by taking only the two segments of the loop of the vortex soliton into account suggested that we should devise a further simplified model, which we shall explain in the next section.
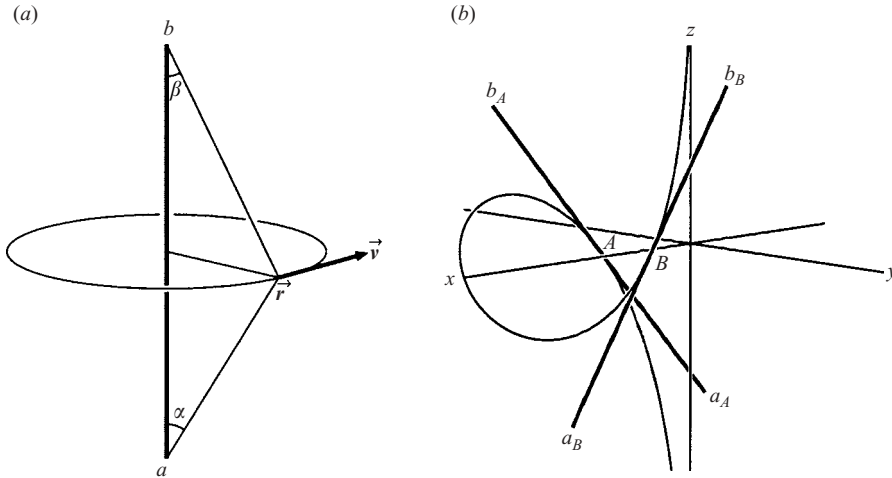
FIGURE 8. (*a*) Velocity induced by a vortex stick of a unit length. The sum of the cosine of the angles between the vertex and the end points appears as a factor in the formula. (*b*) Configuration of a vortex soliton and two chopstick vortices which are tangent to the soliton at $A(x_0, -y_0, 0)$ and $B(x_0, y_0, 0)$.

4. The 'chopsticks' model

As an extension of the truncated model in the last section, we propose a simplified model, in which a loop vortex soliton is replaced with two straight-line vortex segments (chopsticks).

Let us first review the velocity field induced by a straight vortex stick of unit length in three-dimensional space. Of course, this model is meant to simulate a localized effect of a strong vortex and lacks reality because a vortex filament never ends in space owing to the solenoidal condition, div $\boldsymbol{\omega} = 0$.

Suppose one vortex stick with circulation Γ is located as in figure 8(*a*) with the position vector of one end at $\boldsymbol{a}$ and the other at $\boldsymbol{b}$. By denoting the unit direction vector as $\boldsymbol{t}$, the induced velocity at $\boldsymbol{r}$ by the vortex stick is given by

$$\boldsymbol{v}(\boldsymbol{r}) = (\cos\alpha + \cos\beta)\frac{\Gamma}{4\pi}\frac{\boldsymbol{t} \times (\boldsymbol{r} - \boldsymbol{a})}{|\boldsymbol{t} \times (\boldsymbol{r} - \boldsymbol{a})|^2}, \tag{4.1}$$

where $0 < \alpha, \beta < \pi/2$ are angles between the vortex stick and the vertices drawn from $\boldsymbol{r}$ to $\boldsymbol{a}$ and $\boldsymbol{b}$, respectively. We see that the formula gives the same values by replacing the vector $\boldsymbol{a}$ with any point vector on the line vortex. The above expression can be derived by evaluating the Biot-Savart integral by the following integral formula,

$$\int^x \frac{As + B}{(s^2 + ps + q)^{3/2}}\,\mathrm{d}s = 2\frac{(Ap - 2B)s + 2Aq - Bp}{(p^2 - 4q)\sqrt{s^2 + ps + q}}.$$

Notice that if the length of the vortex stick is extended to infinity, the end-effect factor, $\cos\alpha + \cos\beta$, goes to 2, which gives the velocity field by a straight line vortex with infinite length. (We shall eventually use this approximation later.)

Now two vortex sticks are placed in three-dimensional space to model the particle motion. They are arranged to be tangent to the soliton at two points, $A(x_0, -y_0, 0)$ and $B(x_0, y_0, 0)$ (figure 8*b*). (The values of x_0 and y_0 are calculated numerically first by solving $z_f(\sigma) = 0$ for σ in (2.5) and then substitute it to $x_f(\sigma)$ and $y_f(\sigma)$.) For simplicity, we assume that both the sticks have a unit length with the coordinates of

start and end points being

$$\boldsymbol{a}_A = \begin{pmatrix} x_0 - \cos\phi_A \sin\theta_A/2 \\ -y_0 - \sin\phi_A \sin\theta_A/2 \\ -\cos\theta_A/2 \end{pmatrix}, \quad \boldsymbol{b}_A = \begin{pmatrix} x_0 + \cos\phi_A \sin\theta_A/2 \\ -y_0 + \sin\phi_A \sin\theta_A/2 \\ +\cos\theta_A/2 \end{pmatrix},$$

$$\boldsymbol{a}_B = \begin{pmatrix} x_0 - \cos\phi_B \sin\theta_B/2 \\ y_0 - \sin\phi_B \sin\theta_B/2 \\ -\cos\theta_B/2 \end{pmatrix}, \quad \boldsymbol{b}_B = \begin{pmatrix} x_0 + \cos\phi_B \sin\theta_B/2 \\ y_0 + \sin\phi_B \sin\theta_B/2 \\ +\cos\theta_B/2 \end{pmatrix},$$

where the angles $\phi_{A,B}$ and $\theta_{A,B}$ are usual azimuthal and polar angles for tangent vectors, respectively. (i.e. $\theta = 0$: z-axis, $\theta = \pi/2, \phi = 0$: x-axis). (These parameter settings are redundant to determine the configuration of two straight lines in three-dimensional space. We use this settings, however, because we would like to keep the vector expressions of the background rotation and translation simple.) From the symmetry of the vortex soliton, we have the following relations between $\phi_{A,B}$ and $\theta_{A,B}$

$$\begin{cases} \cos\theta_B = \cos\theta_A, \\ \sin\theta_B = \sin\theta_A, \end{cases} \quad \begin{cases} \cos\phi_B = -\cos\phi_A, \\ \sin\phi_B = \sin\phi_A. \end{cases} \tag{4.2}$$

With the above symmetry conditions, the tangent vectors $\boldsymbol{t}_A$ and $\boldsymbol{t}_B$ become

$$\boldsymbol{t}_A = \begin{pmatrix} \cos\phi\sin\theta \\ \sin\phi\sin\theta \\ \cos\theta \end{pmatrix}, \quad \boldsymbol{t}_B = \begin{pmatrix} -\cos\phi\sin\theta \\ \sin\phi\sin\theta \\ \cos\theta \end{pmatrix}. \tag{4.3}$$

Replacing the Biot-Savart integral with (4.1) and substituting the symmetry condition (4.2) into (2.8), we obtain the following model equation for the velocity of a particle at $\boldsymbol{x} = (x, y, z)$. Notice that in the following model equation the end-effect factor is 2 (infinite length approximation), and that the suffices A, B are removed from ϕ and θ.

$$\frac{d}{dt}\begin{pmatrix} x \\ y \\ z \end{pmatrix} = \frac{1}{2\pi}\frac{1}{|\boldsymbol{t}_A \times (\boldsymbol{x} - \boldsymbol{a}_A)|^2}\begin{pmatrix} \sin\phi\sin\theta z - \cos\theta(y + y_0) \\ \cos\theta(x - x_0) - \cos\phi\sin\theta z \\ \cos\phi\sin\theta(y + y_0) - \sin\phi\sin\theta(x - x_0) \end{pmatrix}$$

$$+ \frac{1}{2\pi}\frac{1}{|\boldsymbol{t}_B \times (\boldsymbol{x} - \boldsymbol{a}_B)|^2}\begin{pmatrix} \sin\phi\sin\theta z - \cos\theta(y - y_0) \\ \cos\theta(x - x_0) + \cos\phi\sin\theta z \\ -\cos\phi\sin\theta(y - y_0) - \sin\phi\sin\theta(x - x_0) \end{pmatrix}$$

$$+ (v^2 + \tau^2)G\begin{pmatrix} y \\ -x \\ 0 \end{pmatrix} - 2\tau G\begin{pmatrix} 0 \\ 0 \\ 1 \end{pmatrix}, \tag{4.4}$$

where

$$\begin{aligned} |\boldsymbol{t}_A \times (\boldsymbol{x} - \boldsymbol{a}_A)|^2 = {} & (\cos^2\theta + \sin^2\phi\sin^2\theta)(x - x_0)^2 \\ & + (\cos^2\theta + \cos^2\phi\sin^2\theta)(y + y_0)^2 + \sin^2\theta z^2 \\ & - 2\sin\theta\cos\theta\sin\phi z(y + y_0) - 2\sin\theta\cos\theta\cos\phi(x - x_0)z \\ & - 2\sin\phi\cos\phi\sin^2\theta(x - x_0)(y + y_0) \end{aligned}$$
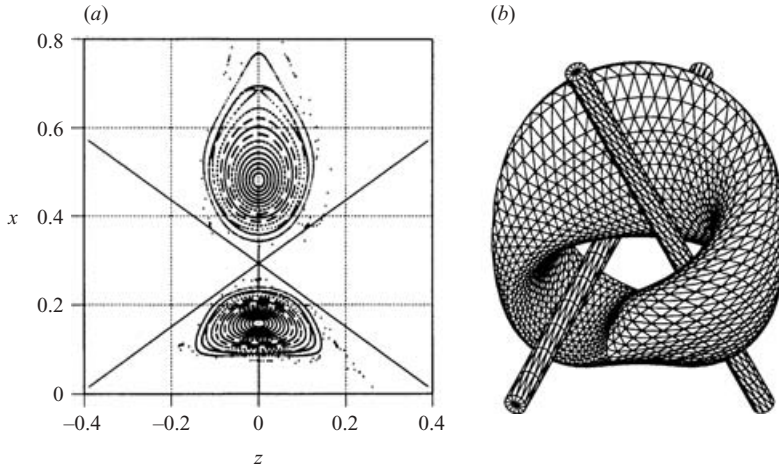
FIGURE 9. Poincaré section and perspective view of a torus made by the chopsticks model (with infinite length).

and

$$|\boldsymbol{t}_B \times (\boldsymbol{x} - \boldsymbol{a}_B)|^2 = (\cos^2 \theta + \sin^2 \phi \sin^2 \theta)(x - x_0)^2$$
$$+ (\cos^2 \theta + \cos^2 \phi \sin^2 \theta)(y - y_0)^2 + \sin^2 \theta z^2$$
$$- 2 \sin \theta \cos \theta \sin \phi z (y - y_0) + 2 \sin \theta \cos \theta \cos \phi (x - x_0) z$$
$$+ 2 \sin \phi \cos \phi \sin^2 \theta (x - x_0)(y - y_0) \,.$$

It should be pointed out that the linearized equation still holds the reversible symmetry by Moser. We can rewrite the right-hand side of the above equation with the aid of a vector potential as

$$\frac{\mathrm{d}}{\mathrm{d}t} \begin{pmatrix} x \\ y \\ z \end{pmatrix} = \nabla \times \left[-\frac{1}{2\pi} \log |\boldsymbol{t}_A \times (\boldsymbol{x} - \boldsymbol{a}_A)| \boldsymbol{t}_A - \frac{1}{2\pi} \log |\boldsymbol{t}_B \times (\boldsymbol{x} - \boldsymbol{a}_B)| \boldsymbol{t}_B \right.$$
$$\left. + \tfrac{1}{2}(\nu^2 + \tau^2) G \begin{pmatrix} 0 \\ 0 \\ x^2 + y^2 \end{pmatrix} + \tau G \begin{pmatrix} y \\ -x \\ 0 \end{pmatrix} \right], \quad (4.5)$$

which may help to understand the chaotic behaviour of the dynamical system (see §5).

By linearizing the stationary solution (2.5) with $(\nu, \tau) = (1.924, 0.3827)$ around $(x_0, y_0, 0)$ where $x_0 = 0.29324$ and $y_0 = 0.111538$, we have

$$\begin{cases} \cos \theta = 0.72761, \\ \sin \theta = 0.68599, \end{cases} \quad \begin{cases} \cos \phi = 0.9897, \\ \sin \phi = -0.156275. \end{cases} \quad (4.6)$$

Figure 9 is the Poincaré section and the three-dimensional view of one torus for particle trajectories calculated with the chopsticks model (4.4). The parameter values are the same as those for the truncated model in figure 7. A similar torus structure is obtained for the original vortex soliton and the truncated model. In the Poincaré section, the primary island of tori is evident, but small secondary islands can also be
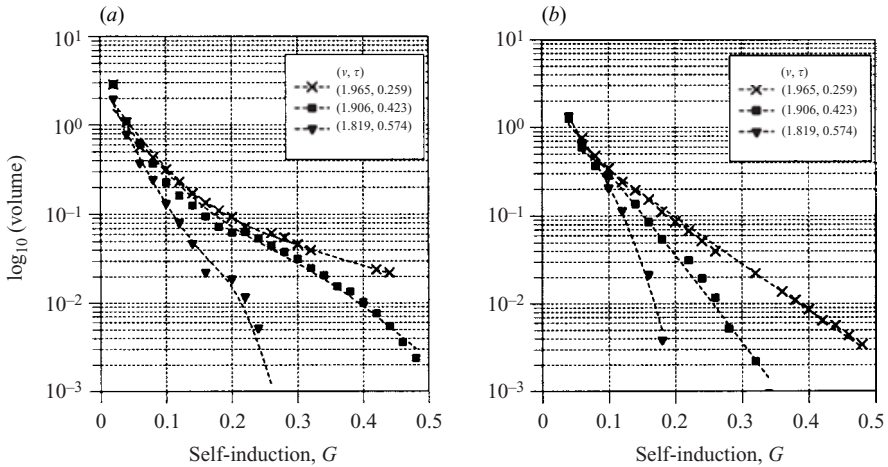
FIGURE 10. Comparison of the volume of the outermost torus as a function of G for three different combinations of ν and τ. (*a*) Vortex soliton (excerpts from figure 5), (*b*) chopsticks model.

observed. The boundary of the torus is extended more in the upper direction than in the truncated model.

The transported volumes for the chopsticks model are calculated for some combinations of parameters and demonstrated as a function of G in figure 10. For comparison, the corresponding plot for the original vortex soliton, which is a subset of figure 5, is added. A similar parametrical tendency is observed for the chopsticks model. We should note that the change in the parameters ν and τ results only in the change of angles between the chopsticks while it provides the change of the three-dimensional shape of the vortex soliton for the original model.

A discrepancy in the transported volume between the chopsticks model and the vortex soliton is observed in figure 10, particularly when the shape of the vortex soliton is almost planar (i.e. $\tau \to 0$). One possible reason for this discrepancy is that most of the segments of the loop would have a similar contribution in the Biot-Savart integral for the planar case. This global feature would be out of the scope of the chopsticks model which concentrates on the local interaction of segments near the crossing point. For the motion of an almost planar vortex soliton, Aref & Flinchem (1984) proposed a model in which a vortex soliton is replaced by a vortex ring and a straight-line filament. This model might work also as a model for the explanation of transport. If the global effect is dominant, we predict that a torus would appear near the centre region of the vortex ring. Keeping this expectation in mind, we plotted the Poincaré section for an almost planar soliton in figure 11. While the edge of the outermost torus extends towards the centre of the ring, the centre of the torus is close to the crossing point of the soliton, and thus we can argue that the torus would be localized enough near the crossing point and that the chopsticks model is still effective. Also it should be noted that the cross-section consists of continuous and dotted lines which correspond to (pseudo) periodic orbits, and no hyperbolic points or chaos are observed. For the numerical reason, this almost planar vortex soliton still has slight but non-zero torsion. It may be interesting to see whether the torus occurs only with periodic orbits in the limit of $\tau \to 0$.
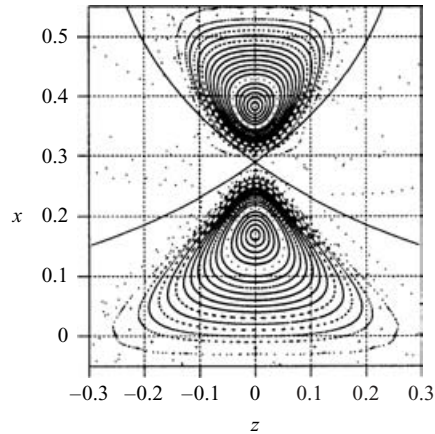
FIGURE 11. Poincaré section for an almost planar loop vortex soliton with $(\nu, \tau, G) = (1.99144, 0.130526, 0.18323)$.

5. Results and discussion

We have demonstrated that a vortex soliton can carry fluid particles inside a domain with a finite volume that makes a knot with the loop of the vortex soliton. Each trajectory of a particle inside the domain forms a surface of a torus with a specific winding number. Groups of tori make a hierarchy of islands, and chaotic trajectories appear near the hyperbolic points between the secondary and higher-order islands. Then, we investigated the transport properties of the vortex soliton by calculating the volume of the domain for various combinations of parameters specifying the shape and the inner core of the soliton. For the analysis of the formation of tori and the transport of volume, we proposed the chopsticks models, which succeeded in reproducing the torus structure and the dependence of the volume on the parameters qualitatively. From the success of the chopsticks model, it may be conjectured that the crossing configuration of the vortex chopsticks is the most fundamental structure for the above phenomena.

In this section, we shall discuss a possible mechanism for producing the chaos in the chopsticks model. The first conventional approach to investigate a given chaotic system may be to search for a decoupling of the system into an integrable part, which produces analytic structures such as a torus, and a perturbing part, which breaks up the circumference of an integrable torus by a mechanism of resonance. Such a scenario works very well, particularly for Hamiltonian systems with two degrees of freedom, and widespread research has been done (Lichtenberg & Liberman 1983; Ottino 1989) Unfortunately, our present model is a three-dimensional dynamical system which shows different aspects from a Hamiltonian system in an even dimensional space. Although there are some mathematical theories for analysing three-dimensional integrable systems (see, for example, Olver 1986), as far as we know, we do not have a canonical tool to extract an integrable part from a given three-dimensional dynamical system. Therefore, our following effort may only look *ad hoc*.

The first idea stems from a belief that any integrable velocity field associated with the chopsticks should be subject to a configuration with a high symmetry. We can see that the azimuthal angle ϕ is small, and it may be natural to treat this quantity as a perturbation parameter.

If we approximate $\cos\phi \sim 1$, $\sin\phi \sim \phi$ and neglect the terms of order ϕ^2 or higher, the right-hand side of (4.4) can be decoupled into unperturbed and perturbing parts,

$$\frac{\mathrm{d}}{\mathrm{d}t}\begin{pmatrix} x \\ y \\ z \end{pmatrix} = \frac{1}{2\pi}\left[\left(\frac{1}{F}+\frac{1}{H}\right)\begin{pmatrix} -\cos\theta y \\ \cos\theta(x-x_0) \\ \sin\theta y_0 \end{pmatrix} + \left(\frac{1}{F}-\frac{1}{H}\right)\begin{pmatrix} -\cos\theta y_0 \\ -\sin\theta z \\ \sin\theta y \end{pmatrix}\right]$$

$$+ \frac{\phi}{2\pi}\left[\left(\frac{G}{F^2}+\frac{K}{H^2}\right)\begin{pmatrix} -\cos\theta y \\ \cos\theta(x-x_0) \\ \sin\theta y_0 \end{pmatrix} + \left(\frac{G}{F^2}-\frac{K}{H^2}\right)\begin{pmatrix} -\cos\theta y_0 \\ -\sin\theta z \\ \sin\theta y \end{pmatrix}\right.$$

$$\left. + \sin\theta\left(\frac{1}{F}+\frac{1}{H}\right)\begin{pmatrix} z \\ 0 \\ -(x-x_0) \end{pmatrix}\right] + (v^2+\tau^2)G\begin{pmatrix} y \\ -x \\ 0 \end{pmatrix} - 2\tau G\begin{pmatrix} 0 \\ 0 \\ 1 \end{pmatrix}, \quad (5.1)$$

where

$$F = (\cos\theta(x-x_0)-\sin\theta z)^2 + (y+y_0)^2,$$
$$G = 2\sin\theta(y+y_0)(\cos\theta z + \sin\theta(x-x_0)),$$
$$H = (\cos\theta(x-x_0)+\sin\theta z)^2 + (y-y_0)^2,$$
$$K = 2\sin\theta(y-y_0)(\cos\theta z - \sin\theta(x-x_0)).$$

As a summary, the unperturbed part corresponds to a situation where two chopsticks are located symmetrically on the planes of $y=\pm y_0$, and the perturbation breaks the symmetry by opening one end of the chopsticks.

The second idea is about the vector potential expression of the dynamical system (4.5). Vector potentials are important in electromagnetic theory, but their roll in characterizing a dynamical system is not obvious. The situation is different from that for a dynamical system with a scalar potential. In fact, if a dynamical system is given in terms of a scalar potential, like $\dot{x} = \nabla f(x)$, the level sets of its solutions are always equi-contour surfaces of the potential $f(x)$. On the other hand, for a vector potential providing an integral of motion, its existence does not necessarily mean reduction of a solution space of any kind. As our example shows, a system with a vector potential may show both integrable or chaotic behaviours.

Another point relating to the vector potential expression is that any solenoidal vector field can be written as a sum of a toroidal and a poloidal vector field about an axis. If we use this fact, any solenoidal dynamical system can be expressed as

$$\frac{\mathrm{d}}{\mathrm{d}t}x = \nabla \times (\phi(x)\hat{z}) + \nabla \times \nabla \times (\psi(x)\hat{z}),$$

where $\phi(x)$ and $\psi(x)$ are scalar functions. (Chandrasekhar & Kendall 1957; Yoshida & Giga 1990) Note that the above expression is a natural extension of the streamfunction expression for two-dimensional solenoidal flows to three-dimensional cases. By changing the combination of the scalar functions, we can have various three-dimensional integrable and chaotic dynamical systems (Arter 1983; Holm & Kimura 1991). Looking at (4.5) from this perspective, we notice that the second and the third terms in the right-hand side can be written as

$$\nabla \times \left[\tfrac{1}{2}(v^2+\tau^2)G(x^2+y^2)\hat{z}\right] + \nabla \times \nabla \times [\tau G(x^2+y^2)\hat{z}], \quad (5.2)$$

where $\hat{z} = {}^t(0,0,1)$, which provide the toroidal and poloidal vector fields. Coupled with the first term which comes from the nonlinear interaction of the two chopsticks,

these background vector field make the flow field complex in a three-dimensional space. The true effect of these background flow must be analysed.

Lastly, we would like to make a comment on the reversible symmetry which both the original equation and the chopsticks model satisfy. Moser (1973) showed the possibility of a discussion about the non-integrability of systems with reversible symmetry. He presented a theorem similar to the KAM theory for an even-dimensional reversible system. We understand that applicability of the theorem to odd-dimensional systems such as the models in this paper is still an open problem.

So far, we can demonstrate that a vortex soliton, which is a one-class solution for the motion of a vortex filament without changing its shape by Kida (1981), can transport a fluid volume. As the next stage of the problem, it may be of interest to study particle transport by other types of solitary wave (Maxworthy, Hopfinger & Redekopp 1985) and unsteady interacting waves on a vortex filament (Aref & Flinchem 1984). We hope that the chopsticks model might give some insights into the mechanism of particle transport in those problems.

Advection of particles by a vortex soliton, may be classified as an example of three-dimensional chaotic advection (Aref 1984, 2002). The characteristic idea of chaotic advection can be described by a statement that 'even an integrable Eulerian flow field can produce chaotic motions for Lagrangian particles', which captures the feature of our subject well. If we notice, however, that the Eulerian flow field is particularly generated by a soliton, and that the advected volume has compact topological properties which are subject to the shape of the soliton, we may call this problem especially 'soliton advection.'

REFERENCES

AREF, H. 1984 Stirring by chaotic advection. *J. Fluid Mech.* **143**, 1–21.

AREF, H. 1991 Stochastic particle motion in laminar flows. *Phys. Fluids* A **3**, 1009–1016.

AREF, H. 2002 The development of chaotic advection. *Phys. Fluids* **14**, 1315–1325.

AREF, H. & FLINCHEM, E. P. 1984 Dynamics of a vortex filament in a shear flow. *J. Fluid Mech.* **148**, 477–497.

ARTER, W. 1983 Ergodic stream-lines in steady convection. *Phys. Lett.* A **97**, 171–174.

BATCHELOR, G. K. 1956 On steady laminar flow with closed streamlines at large Reynolds number. *J. Fluid Mech.* **1**, 177–190.

BATCHELOR, G. K. 1967 *An Introduction to Fluid Dynamics.* Cambridge University Press.

CHANDRASEKHAR, S & KENDALL, P. C. 1957 On force-free magnetic fields. *Astrophys. J.* **126**, 457–460.

GRIMSHAW, R. 1990 *Nonlinear Ordinary Differential Equations.* Blackwell.

HAMA, F. R. 1962 Progressive deformation of a curved vortex filament by its own induction. *Phys. Fluids* **5**, 1156–1162.

HAMA, F. R. 1963 Progressive deformation of a perturbed line vortex filament. *Phys. Fluids* **6**, 526–534.

HASIMOTO, H. 1972 A soliton on a vortex filament. *J. Fluid Mech.* **51**, 477–485.

HOLM, D. D. & KIMURA, Y. 1991 Zero-helicity Lagrangian kinematics of three-dimensional advection. *Phys. Fluids* A **3**, 1033–1038.

HOPFINGER, E. J. & BROWAND, F. K. 1982 Vortex solitary waves in a rotating, turbulent flow. *Nature* **295**, 393–395.

HOPFINGER, E. J., BROWAND, F. K. & GAGNE, Y. 1982 Turbulence and waves in a rotating tank. *J. Fluid Mech.* **125**, 505–534.

KIDA, S. 1981 A vortex filament moving without change of form. *J. Fluid Mech.* **112**, 397–409.

KIMURA, Y. 1989 Transport properties of waves on a vortex filament. *Physica* D **37**, 485–489.

KONNO, K. & ICHIKAWA, Y. H. 1995 Strong interference of sound pressure generated by vortex soliton with axial flow. *Chaos Solitons, Fractals* **5**, 2485–2493.

KRAICHNAN, R. H. 1970 Diffusion by a random velocity field. *Phys. Fluids* **13**, 22–31.

LAMB, G. L. 1980 *Elements of Soliton Theory*. Wiley.

LEONARD, A. 1985 Computing three-dimensional incompressible flows with vortex elements. *Annu. Rev. Fluid Mech.* **17**, 523–559.

LICHTENBERG, A. J. & LIEBERMAN, M. A. 1983 *Regular and Stochastic Motion*. Springer.

MAJDA, A. 1991 Vorticity, turbulence, and acoustics in fluid flow. *SIAM Rev.* **33**, 349–388.

MAXWORTHY, T., HOPFINGER, E. J. & REDEKOPP, L. G. 1985 Wave motions on vortex cores. *J. Fluid Mech.* **151**, 141–165.

MOSER, J. 1973 *Stable and Random Motions in Dynamical Systems with Special Emphasis on Celestial Mechanics*. Princeton University Press.

NEWTON, P. K. 2001 *The N-Vortex Problem, Analytical Techniques*. Springer.

OLVER, P. J. 1986 *Applications of Lie Groups to Differential Equations*. Springer.

OTTINO, J. M. 1989 *The Kinematics of Mixing: Stretching, Chaos, and Transport*. Cambridge University Press.

RHINES, P. B. & YOUNG, W. R. 1983 How rapidly is a passive scalar mixed within closed streamlines? *J. Fluid Mech.* **133**, 133–145.

RICCA, R. L. 1991 Rediscovery of DaRios equations. *Nature* **352**, 561–562.

SAFFMAN, P. G. 1992 *Vortex Dynamics*. Cambridge University Press.

YOSHIDA, Z. & GIGA, Y. 1990 Remarks on spectra of operator rot. *Math. Z.* **204**, 235–245.